

PointDreamer: Zero-shot 3D Textured Mesh Reconstruction from Colored Point Cloud by 2D Inpainting

Qiao Yu¹ Xianzhi Li^{1†} Yuan Tang¹ Jinfeng Xu¹ Long Hu¹ Yixue Hao¹ Min Chen²

¹ Huazhong University of Science and Technology ² South China University of Technology

[†] Corresponding author

{qiaoyu_epic, xzli, yuan_tang}@hust.edu.cn jinfengxu.edu@gmail.com,
{hulong, yixuehao}@hust.edu.cn, minchen@ieee.org

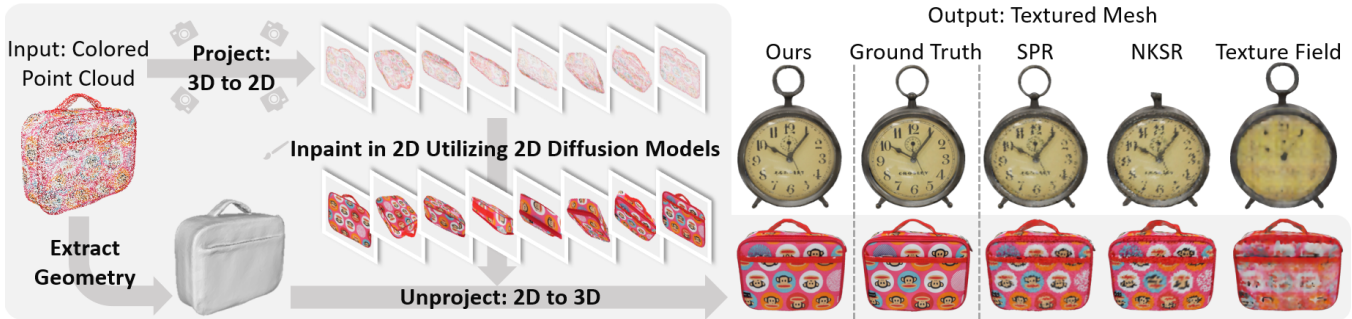


Figure 1: PointDreamer is a zero-shot framework to reconstruct 3D textured meshes from colored point clouds. The key idea is to utilize 2D diffusion priors to inpaint the projected 2D multi-view sparse images to dense ones, which are finally unprojected back to 3D to produce mesh textures. PointDreamer produces textures with enhanced clarity compared to various competitors, such as Screened Poisson Reconstruction (SPR) [21], Neural Kernel Surface Reconstruction (NKSR) [17], and Texture Field [37].

ABSTRACT

Reconstructing textured meshes from colored point clouds is an important but challenging task in 3D graphics and vision. Most existing methods predict colors as implicit functions in 3D or UV space, suffering from blurry textures or the lack of generalization capability. Addressing this, we propose PointDreamer, a novel framework for textured mesh reconstruction from colored point cloud. It produces meshes with enhanced fidelity and clarity by 2D image inpainting, taking advantage of the mature techniques and massive data of 2D vision. Specifically, we first project the input point cloud into 2D space to generate sparse multi-view images, and then inpaint empty pixels utilizing a pre-trained 2D diffusion model. Next, we design a novel Non-Border-First strategy to unproject the colors of the inpainted dense images back to 3D space, thus obtaining the final textured mesh. In this way, our PointDreamer works in a zero-shot manner, requiring no extra training. Extensive qualitative and quantitative experiments on various synthetic and real-scanned datasets show the SoTA performance of PointDreamer, by significantly outperforming baseline methods with 30% improvement in LPIPS score (from 0.118 to 0.068). Code at: <https://github.com/YuQiao0303/PointDreamer>.

CCS CONCEPTS

• **Computing methodologies** → **Reconstruction**: 3D imaging; Shape representations; **Appearance and texture representations**; Shape inference.

KEYWORDS

3D Textured Mesh, Colored Point Cloud Reconstruction, Diffusion Models, Image Inpainting

1 INTRODUCTION

3D textured mesh reconstruction from colored point cloud is a pivotal task in computer vision, graphics and robotics. It enables the transition from sparse and unstructured point clouds to connected and visually-appealing meshes, facilitating applications like digital twin [51], metaverse [54], cultural heritage preservation [53], etc.

With the great success achieved in geometry reconstruction by learning a 3D implicit field like signed distance field (SDF) [38], occupancy field [6, 33], etc., researchers propose to learn a 3D texture field [37] representing color information in 3D space. Nevertheless, such approaches often yield blurry appearances [48]. In addition, they necessitate 3D data for training, which is notoriously challenging to acquire, and the limited training data further hinder the models' generalization capability to unseen objects.

While the 3D textured mesh reconstruction task remains challenging, 2D vision has recently witnessed great prosperity in the field of image super-resolution and image generation, particularly thanks to the emergence of diffusion models [15]. Compared to 3D vision, 2D vision is more mature, and the abundance of 2D data offers a robust prior, which has been proven crucial for enhancing the performance and generalization ability of deep learning models [36, 42]. Inspired by this, numerous studies [25, 27, 28, 40, 41, 49] seek to adopt 2D diffusion models as a prior to guide 3D generation, mostly by optimizing a score distillation sampling (SDS) [40]

loss or reconstruction loss between the generated 3D models’ rendered images and 2D diffusion models’ output images. However, they focus on text/image/un-conditioned 3D generation, leaving point-cloud-based reconstruction unexplored. Besides, the colors or textures are still learned or optimized in 3D space (as a texture field or radiance field), yielding blurry appearances [48].

Going beyond existing approaches, our intuition is that, reconstructing 3D textured meshes from colored point clouds is analogous to inpainting 2D sparse images by filling empty pixels. Both tasks focus on somehow *dreaming* the missing areas of the sparse input, to achieve a more complete and coherent representation. Intuitively, dreaming in 2D space is much easier than in 3D space, especially with powerful tools like diffusion models. This inspires us to convert the dreaming process into 2D space to enhance reconstruction quality especially clarity, and then reconvert the results back to 3D. Specifically, unlike existing works [9, 29, 40, 45] that learns per-point colors as implicit functions in 3D space, we predict per-pixel colors in 2D image space by 2D image inpainting, and then directly unproject the high-quality results back to 3D space, so as to generate clear textures for meshes.

Guided by this idea, we design *PointDreamer*, a novel zero-shot framework for reconstructing high-quality textured meshes from colored point clouds, as shown in Figure 1. With only a set of pre-defined camera parameters from different viewpoints, an off-the-shelf 2D diffusion model, and a geometry extraction module, our method starts from projecting the input point cloud into 2D to generate multi-view sparse images. The 2D diffusion model is then adopted to inpaint the sparse images into dense ones. Finally, we unproject the colors of dense images back to obtain the 3D textured mesh by a carefully-designed *Non-Border-First* unprojection strategy. It prioritizes non-border areas during unprojection, to circumvent inaccurate color prediction at occlusion borders and thus avoid artifacts. Overall, we list our contributions as follows:

- We propose PointDreamer, a **zero-shot** framework for 3D textured mesh reconstruction from colored point cloud. By novelly transforming this 3D reconstruction task into 2D inpainting, PointDreamer achieves **high-fidelity appearance** and **strong generalization ability** while **requiring no extra training**, and pioneers in utilizing 2D diffusion models for 3D point cloud reconstruction.
- We design Non-Border First (NBF) Unprojection, a novel unprojection strategy for 2D-to-3D re-conversion that effectively avoids artifacts caused by inaccurate color prediction near occlusion borders.
- Experiments on various benchmarks show the SoTA performance of PointDreamer, by significantly outperforming baseline methods both quantitatively and qualitatively.

2 RELATED WORK

2.1 Textured Mesh Reconstruction from Colored Point Cloud

While many works [2, 33, 39, 47] focus on reconstructing surfaces from non-colored point clouds, textured mesh reconstruction from colored point cloud remains a field to be further explored. Traditionally, (Screened) Poisson Surface Reconstruction (SPR) [20, 21] reconstructs textured meshes by solving the Poisson equation, but it relies

on accurate per-point normals as input. In contrast, DHSP3D [57] optimizes a MeshCNN in 3D space and XYZ/RGB maps in 2D UV space by self-supervision, but it does not support arbitrary topology. Recently, a more common practice [13, 17] is to learn two 3D implicit fields or hyper-representations for geometry and texture, respectively. For geometry reconstruction, Signed Distance Field (SDF) [13], Occupancy Field [5], Neural Kernel Field [17], Deep Marching Tetrahedra (DMTet) [13, 43], etc. are optional shape representations to be learned or optimized. For texture reconstruction, a texture field [37] consisting of separated functions for red, green and blue channels is generally fitted, supervised by MAE loss for per-point color [5, 17] or reconstruction loss [13] for images from differentiable rendering. Unfortunately, such methods without powerful prior often suffer from relatively blurry texture [22]. To address this, we are the first, to the best of our knowledge, to perform the 3D reconstruction task by 2D inpainting to take advantage of existing high-performance 2D vision techniques.

2.2 Representations of Colored 3D Objects

Researchers have explored various ways to represent 3D objects or scenes with colors. To begin with, CMR [18] and its followers [11, 16, 24, 60] regard a shape as the deformation of a sphere with fixed UV mapping, thus only supporting spherical topology. Unlike them, NeRF variants [1, 34, 35] or DMTet [43] with texture field [37] have shown their advantages in representing power and generation quality [4, 9, 27–29, 40, 46, 50] thanks to the techniques of volumetric rendering and differentiable rendering [23]. Recently, 3D Gaussian Splatting [22] has drawn considerable attention where 3D scenes are represented as a set of 3D Gaussians. However, as mentioned before, learning or optimizing colors in 3D space often results in blurry textures [48]. In contrast, we directly predict high-fidelity colors in 2D image space by utilizing the power of a 2D pre-trained diffusion model, which can be further unprojected to 3D meshes to obtain clearer textures.

2.3 Diffusion Models for 3D Shape Generation

With the success of 2D diffusion models, researchers have explored extending applications of diffusion models to 3D field. An intuitive idea is to apply the diffusion process on 3D representations, such as a DMTet grid [30], occupancy or SDF field [62], or 3D feature triplane [13]. To fully capitalize on the abundant availability of 2D data, more researchers seek to directly “lift” results of 2D diffusion models to 3D. Most of these works [4, 9, 25–29, 32, 40, 41, 44, 46, 49, 50] optimize a NeRF, a DMTet or 3D Gaussians by SDS [40] or reconstruction loss to make the generated 3D scene similar to the result of a given 2D diffusion model (e.g. Stable-Diffusion). View-conditioned diffusion models [28] or multi-view diffusion models [29, 46] are developed by fine-tuning existing models for generating multi-view-consistent images. Most of these works still learn or optimize colors in 3D space. They tend to be time-consuming during optimization, and suffer from relatively blurry results in unseen views. Instead of optimizing a 3D representation from scratch to follow the images generated by 2D diffusion models, we propose to directly adopt colors of the 2D images, by unprojecting them back to 3D, for higher-quality texture reconstruction.

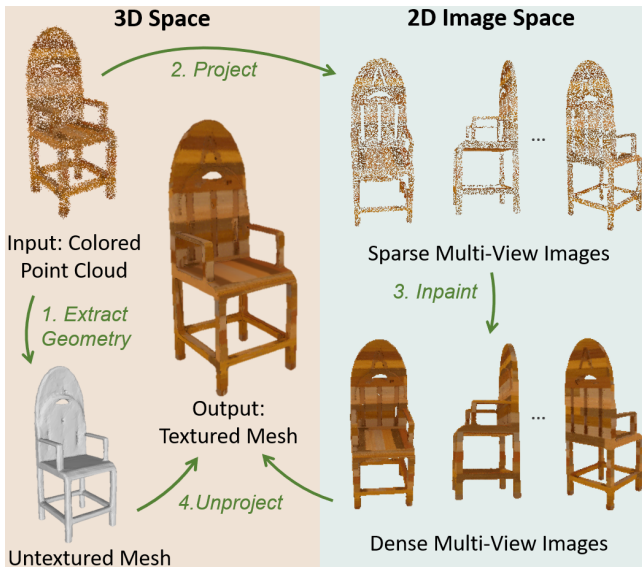


Figure 2: Pipeline of our method. Given a colored point cloud, we first reconstruct its untextured mesh. Then, the colored point cloud is projected to 2D to produce sparse multi-view images, which are further inpainted to form the dense ones. Finally, we unproject the results back to 3D to output the associated textured mesh.

3 METHOD

Given a 3D point cloud with per-point XYZ coordinates and RGB colors, our goal is to reconstruct its associated textured mesh. Unlike existing works that learn or optimize colors in 3D space [37, 40] or UV space [5, 57], we propose PointDreamer, a novel approach by conducting color prediction in 2D image space to leverage the powerful 2D diffusion priors. Figure 2 presents our designed pipeline with four steps. First, we employ a geometry extraction module to reconstruct an untextured mesh from the input point cloud. Next, with a set of fixed viewpoints, we perform 3D-to-2D conversion by projecting the input point cloud into 2D, producing sparse multi-view images. After that, we conduct color prediction in 2D space by inpainting the empty pixels in the sparse images to form dense ones based on a pre-trained 2D diffusion model [7]. Finally, we propose a novel Non-Border-First strategy to convert the 2D results back to 3D by unprojecting the colors in the dense images to the untextured mesh to produce the desired textured mesh. Note that with the 2D diffusion priors, our method is zero-shot requiring no extra training on 3D datasets.

3.1 Geometry Extraction: Point to Surface

The first step in PointDreamer is to reconstruct an untextured mesh from the input point cloud. Since color information does not need to be considered in this step, many existing point-to-surface methods [2, 33, 39, 43] can be employed. In our implementation, we directly adopt the state-of-the-art POCO [2] considering its high performance. Section 4 provides ablation experiments by using different geometry reconstruction methods.

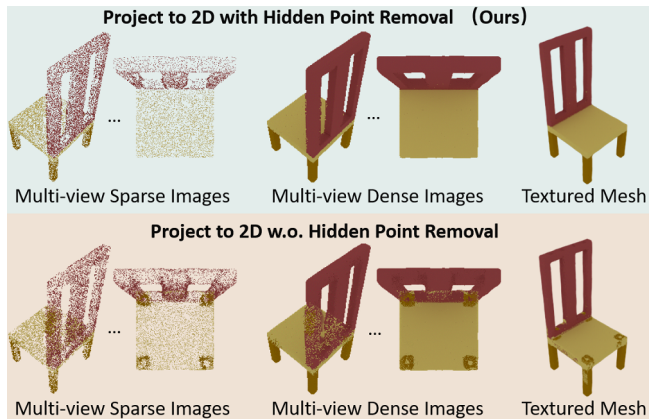


Figure 3: Illustration of hidden point removal, without which the results would be messed up.

3.2 Projection and Inpainting

As shown in Figure 2, we design a projection module for 3D-to-2D conversion, followed by an inpainting module for 2D color prediction by inpainting sparse multi-view images into dense ones.

3.2.1 Projection: 3D to 2D. Directly projecting the whole point cloud into 2D would incorporate points from occluded parts that should not be visible from the given view. This would mess up the inpainting results and subsequent mesh textures; see the bottom of Figure 3 as an example. Therefore, before generating the sparse images, we preprocess the input point cloud by the “Hidden Point Removal” operator [19], which works by transforming the input and extracting the points that reside on its convex hull. With pre-set camera parameters of K viewpoints ($K = 8$ in our implementation) and associated visible point clouds, we conduct camera transformation to these points to get their corresponding pixel coordinates in 2D image space. These pixels are painted according to their associated 3D points’ colors, producing K sparse images. Comparisons of different K values can be found in our supplementary file.

3.2.2 Inpainting: Sparse to Dense. Any 2D inpainting method that fills empty pixels in input images can serve as our inpainting module. We propose to use the state-of-the-art DDNM [55] based on a pre-trained unconditional 2D diffusion model [7] to inpaint the multi-view sparse images into dense ones $\mathbf{I} = \{I_k\}_{k=1}^K$. In this way, the strong prior provided by the 2D diffusion model can facilitate high-quality inpainting. So far, we have completed color prediction purely in 2D space instead of 3D or UV space.

3.3 Unprojection: 2D to 3D

With color prediction conducted in 2D space, we now need to convert the result back to 3D. Specifically, the goal is to use the extracted untextured mesh and inpainted multi-view posed images, to generate the associated textured mesh. Regarding this, we design a novel approach namely “Non-Border-First Unprojection”.

The top of Figure 4 illustrates the basic idea of the unprojection module. As can be seen, we represent mesh texture as a texture atlas \mathcal{T} by applying UV mapping to a mesh \mathcal{M} via Xatlas [59],

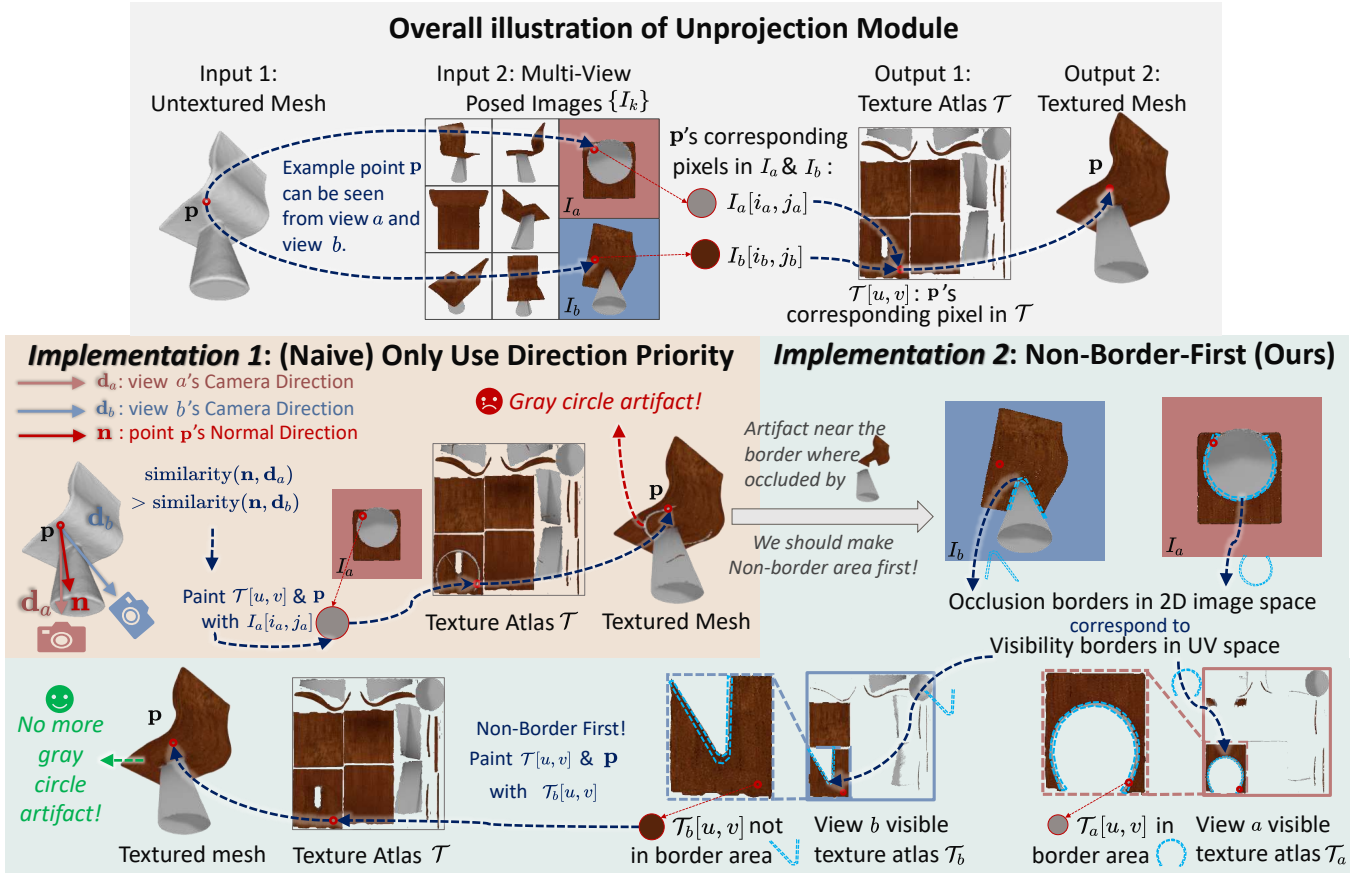


Figure 4: *Top*: Illustration of input and output of the unprojection module, which unprojects colors of 2D multi-view images to a 3D mesh. *Middle Left*: An naive unprojection implementation. For each 3D point p , from all views where p is visible, the highest-direction-priority view is chosen to paint p . Example point p 's corresponding pixel in the selected view a is with inaccurate color since it's near an occlusion border, producing an artifact. *Bottom Right*: our proposed Non-Border-First Unprojection. Observing the correspondence between occlusion border in 2D image space and visibility in UV space (both marked by sky blue dashed lines), we prioritize non-border-areas in UV space to avoid such artifacts.

following [9, 31]. A texture atlas is an RGB image containing different charts. Each chart is a continuous area in UV space that corresponds to a continuous segment of \mathcal{M} in 3D space. Each pixel $\mathcal{T}[u, v]$ of a chart corresponds to a surface point p of \mathcal{M} . Therefore, our goal is to assign a color for each chart pixel $\mathcal{T}[u, v]$. Given a set of multi-view posed images $I = \{I_k\}_{k=1}^K$, p can be seen in zero, one, or more images. If p is visible in I_k , we denote I_k 's corresponding pixel as $I_k[i_k, j_k]$. See the top of Figure 4 as an example, where a 3D point p is visible in two views a and b , and we mark it with a red circle together with its corresponding multi-view image pixels $I_a[i_a, j_a]$, $I_b[i_b, j_b]$, and texture atlas pixel $\mathcal{T}[u, v]$.

Point p 's visibility in view k can be calculated by whether its depth value is no bigger than the corresponding pixel of the k 's depth map. If p is visible only in one view, the corresponding color of $I_k[i_k, j_k]$ can be directly adopted as the color of p and $\mathcal{T}[u, v]$. If p can be seen in no view at all, we can set some rules to deal with it. If p can be seen in more than one view, we can try to fuse the corresponding colors or select one best view. Various unprojection

strategies differ in how to fuse views or select the best view. Here we introduce three implementations for unprojection.

3.3.1 Naive Unprojection: Only Use Direction Priority. An intuitive idea to pick the best view for p or $\mathcal{T}[u, v]$ is by direction priority, as shown in the middle left part of Figure 4. Specifically, for each view k where point p can be seen, we calculate the direction priority score $s_p(k)$, defined as the cosine similarity of p 's normal direction n and view k 's camera direction d_k . The view with the highest direction priority is chosen to paint p and $\mathcal{T}[u, v]$. For example, in the middle left part of Figure 4, p is painted to gray according to $I_a[i_a, j_a]$ since view a has a higher direction priority. Also, if there are a few points invisible from any view, we can still assign a view by direction priority.

While this naive unprojection strategy serves adequately for most points, it produces artifacts under certain circumstances; see again the middle left part of Figure 4, where a gray artifact is visible in the reconstructed textured mesh that should have been brown. Through analysis, such artifacts appear in *border areas*, that is, the

area near the border of occluded (e.g. bottom side of the brown seat in Figure 4) and occluding part (e.g. the gray bottom of the chair) of the shape in a posed image I_k when the former is occluded by the latter from view k (e.g. view a). In such areas, the inpainting module may inaccurately delineate the boundary separating the two parts, e.g. too large gray bottom in view a , resulting in artifacts.

3.3.2 Optimization-based Unprojection. Instead of selecting one single view by direction priority, 3D generation method Dream-Gaussian [48] adopts an optimization-based unprojection strategy to get the textured mesh from multi-view images. The idea is to optimize the texture atlas by the multi-view per-pixel loss between the inpainted multi-view images $\{I_k\}_{k=1}^K$ and the rendered images of the reconstructed textured mesh. In this way, the optimization process kinds of *fuses* corresponding colors in different views instead of selecting the best one. However, it cannot ignore the inaccurate colors in the *border areas*, so the artifacts can only be reduced instead of eliminated. This inspires us to design a non-border-first strategy to address this issue.

3.3.3 Non-Border-First Unprojection (NBF). The bottom of Figure 4 illustrates the idea of our proposed novel unprojection strategy namely Non-Border-First Unprojection, which begins with detecting *border areas* in multi-view images, so as to paint the texture atlas while ignoring them. After that, if some atlas pixels remain unpainted since their associated 3D points can not be seen from any non-border area, we then select from all areas, whether they are border areas or not, to paint the rest pixels. Now the question is, how to accurately detect *border areas*.

Interestingly, we find that, the borders between occluded and occluding parts of the shape in image I_k (2D space) often correspond to the borders between visible and invisible areas in “view k visible texture atlas \mathcal{T}_k ” (UV space), where \mathcal{T}_k is defined as a texture atlas in which only visible areas in view k are filled and rest invisible areas are empty. See the bottom of Figure 4 as an example, where such border areas are marked by sky blue dashed lines. In posed images I_a and I_b , these areas divide the occluded brown seat and the occluding gray bottom, while in view a and b visible texture atlas \mathcal{T}_a and \mathcal{T}_b , these areas divide the visible (painted) and invisible (transparent) parts in view a and b , respectively. The reason for this correspondence of UV visibility border and 2D occlusion border is that, a continuous area within a chart of the texture atlas usually corresponds to a continuous segment of the 3D surface. When a chart contains both visible and invisible regions in a given view k , it often indicates that the corresponding 3D areas of invisible regions are occluded by some other part of the shape. Therefore, we design our Non-Border-First unprojection strategy as follows.

- (1) We paint “view k visible texture atlas map” \mathcal{T}_k for each view k defined as above.
- (2) We calculate the border areas by dilating the edges between visible and invisible areas in \mathcal{T}_k given a certain dilation kernel size as a hyperparameter.
- (3) We paint the final texture atlas \mathcal{T} considering only non-border areas in \mathcal{T}_k . During this, if a point is visible in more than one view’s non-border-areas, we select the best view with the highest direction priority.

- (4) If there remain some unpainted pixels in \mathcal{T} , we now check the previously ignored border areas to paint them, during which we still select among views by direction priority.
- (5) If some points cannot be seen from either view, we assign it with a view by direction priority considering all areas in all views whether they’re border areas or not.
- (6) We experimentally find that additionally optimizing from the generated texture atlas by only calculating the loss of non-border pixels would further enhance the performance.

In this way, our non-border-first strategy can reasonably eliminate artifacts caused by inaccurate color prediction in border areas. We conduct experiments to verify the effectiveness of our proposed strategy in Section 4.

4 EXPERIMENTS AND RESULTS

4.1 Experimental Settings

4.1.1 Datasets. To evaluate the performance of our method against other competitors, we use three benchmark datasets in our experiments.

(i) **ShapeNetCoreV2** [3]: A large-scale synthesis 3D object dataset, where we follow [9] to use the official test splits of *chair*, *car*, and *motorbike* categories for evaluation since they contain relatively complex textures. The test sets of the three categories contain around 1300, 690 and 70 samples, respectively.

(ii) **Google Scanned Objects (GSO)** [8]: A real-scanned 3D object dataset and we use all its 1030 samples for evaluation unlike existing works [29, 31] that only use 30 of them.

(iii) **OmniObject3D** [58]: A real-scanned 3D object dataset with 6000 samples. For efficiency, we randomly select 100 objects for evaluation.

For each textured mesh from the above datasets, we sample 30000 colored points as input. Note that, our approach works in a zero-shot manner, which can be directly applied to objects from various datasets or categories, requiring no extra training but only an off-the-shelf 2D diffusion model [7].

4.1.2 Metrics. To evaluate the quality of the reconstructed 3D textured mesh, we follow existing works [28, 29, 31, 60] to compare the similarity between multi-view images rendered by the reconstructed mesh and ground-truth mesh. Specifically, we render 20 multi-view images on each mesh for a thorough assessment and four similarity metrics are calculated: Peak Signal-to-Noise Ratio (PSNR), Structural Similarity Index Measure (SSIM) [56], Learned Perceptual Image Patch Similarity (LPIPS) [61], and Fréchet Inception Distance (FID) [14]. PSNR measures pixel-level similarity. SSIM considers both pixel values and structural information. LPIPS uses a pre-trained deep neural network to assess image similarity, imitating human perception better than PSNR and SSIM. FID measures the statistical distance between the distribution of two datasets. PSNR and SSIM scores indicate higher quality as their values increase, whereas lower values of LPIPS and FID reflect better performance.

4.2 Baselines

To fully evaluate the performance of our method, we compare it with three kinds of baselines:

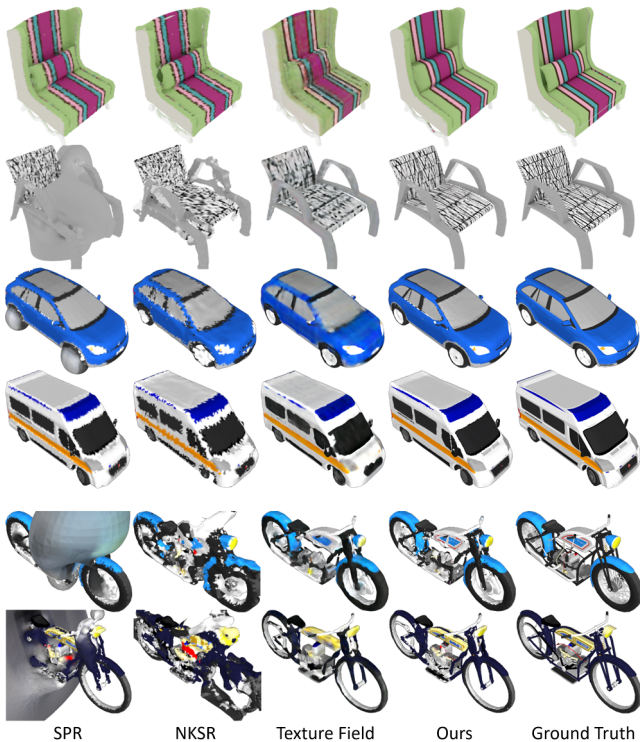


Figure 5: Qualitative results of textured mesh reconstruction on ShapeNetCoreV2 dataset.

(1) *Non-deep-learning method*: We choose the classical Screened Poisson Reconstruction (SPR) [21] for comparison. Note that SPR requires per-point normal as input, and we estimate it via Principal Component Analysis (PCA).

(2) *DHSP3D [57] and NKSR [17]*: These are two recent networks for textured mesh reconstruction and we employ the official code provided by the authors. Similar to SPR, NKSR also requires point normals as additional input.

(3) *Texture Field [37]*: Since we cannot find any existing open-source texture-field-based method requiring only colored point clouds as input, we thus design a baseline network inspired by [13]. The key idea is to learn a 3D feature tri-plane from the input point cloud and then decode RGB values for the query points. We train it on the official training split of the mentioned three categories of ShapeNetCoreV2, supervised by per-point color MSE loss following [13]. During inference, we employ the above-mentioned POCO [2] to reconstruct untextured meshes and utilize our trained texture field network to infer textures by querying colors for the associated 3D point of each texture atlas pixel. In this way, both our proposed PointDreamer and the texture field baseline adopt the same geometry module for a fair comparison. Please refer to our supplementary file for more details about the training and inference of our texture field baseline.

4.3 Main Results

4.3.1 Qualitative comparisons. Since DHSP3D is much slower than other methods (about 4-6 hours per shape compared to < 2 min),

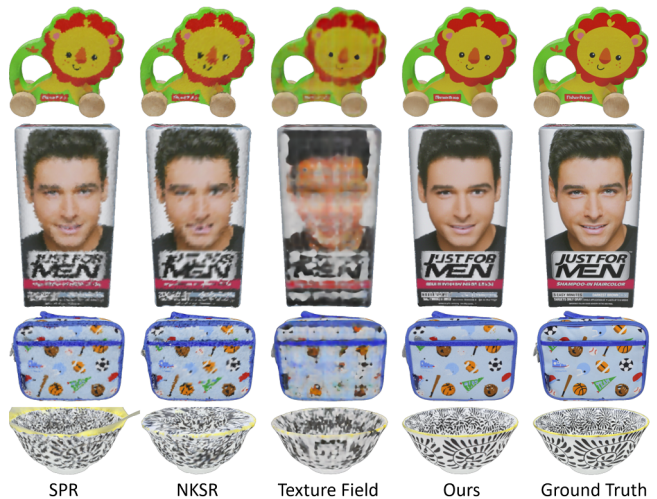


Figure 6: Qualitative results of textured mesh reconstruction on Google Scanned Objects dataset.

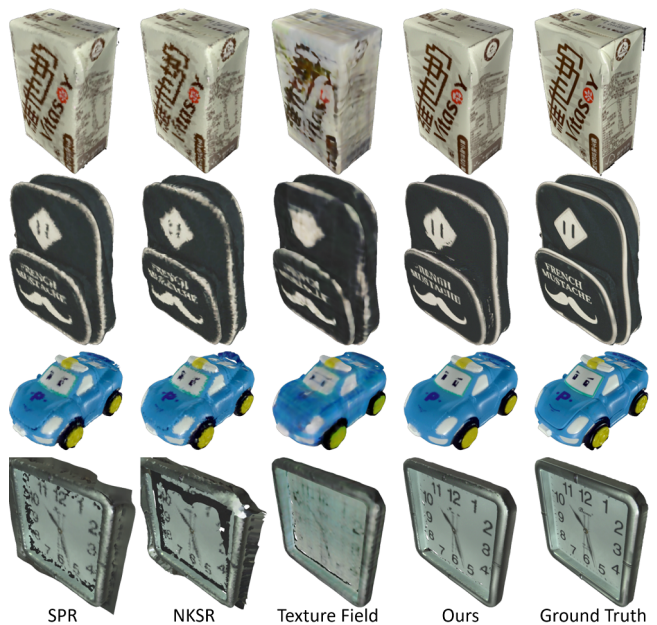


Figure 7: Qualitative results of textured mesh reconstruction on OmniObject3D dataset.

we randomly select two objects from GSO dataset for efficiency when comparing our method against DHSP3D; see Figure 8. For other methods (i.e., SPR, NKSR & texture field), we present the visual comparisons on each dataset separately; see Figures 5, 6 and 7.

Figures 5- 7 show that our method, though zero-shot, achieves much clearer and more realistic textures than baselines, thanks to the strong 2D diffusion prior. Besides, SPR and NKSR, which both rely on per-point normals as input, sometimes yield redundant geometry mainly due to the wrongly-estimated normal direction.



Figure 8: Qualitative results on textured mesh reconstruction comparing our method and DHSP3D.

Table 1: Comparisons on textured mesh reconstruction performance on ShapeNetCoreV2 dataset.

ShapeNet Cat.	Method	PSNR \uparrow	SSIM \uparrow	LPIPS \downarrow	FID \downarrow
Chairs	SPR	24.10	0.931	0.0923	12.03
	NKSR	23.05	0.931	0.0964	29.11
	T.F.	26.12	0.947	0.0664	6.83
	Ours	26.29	0.952	0.0570	4.90
Cars	SPR	23.46	0.929	0.0882	43.89
	NKSR	21.01	0.919	0.0961	131.05
	T.F.	22.42	0.919	0.0868	38.08
	Ours	22.78	0.930	0.0727	12.41
Motorbikes	SPR	15.09	0.809	0.2139	106.09
	NKSR	18.13	0.905	0.1008	175.42
	T.F.	21.17	0.926	0.0635	40.06
	Ours	21.20	0.930	0.0562	28.42

Table 2: Comparisons on textured mesh reconstruction performance on GSO and Omniobject3D datasets. “T.F” denotes Texture Field.

Dataset	Method	PSNR \uparrow	SSIM \uparrow	LPIPS \downarrow	FID \downarrow
GSO	SPR	27.11	0.907	0.1200	27.43
	NKSR	24.65	0.900	0.1184	36.51
	T.F.	25.53	0.894	0.1276	46.44
	Ours	27.24	0.923	0.0827	9.32
OmniObject3D	SPR	30.20	0.927	0.0998	40.13
	NKSR	26.77	0.919	0.1048	50.14
	T.F.	28.08	0.914	0.1121	65.61
	Ours	29.78	0.941	0.0683	18.23

The texture field baseline, which is trained on ShapeNetCoreV2, performs much worse on the newly-seen dataset of GSO and Omniobject3d, indicating a lack of generalization ability.

In Figure 8, the red cup in the first row shows that DHSP3D does not support arbitrary topology. This is because it optimizes meshCNN and 2D XYZ map from the convex hull of the input point cloud, enforcing the output mesh to adhere to the hull’s topology. Besides, DHSP3D suffers from less realistic textures with jagged or unclear edges, since its purely self-prior property only enables it to predict point colors considering corresponding neighbors, without the ability to *dream* the unseen like our PointDreamer.

Table 3: Comparisons on anti-noise ability on chair category of ShapeNetCoreV2 dataset. “Noisy” denotes adding Gaussian noise with a standard deviation of 0.005 to the input point cloud.

Method	PSNR \uparrow		SSIM \uparrow		LPIPS \downarrow		FID \downarrow	
	Clean	Noisy	Clean	Noisy	Clean	Noisy	Clean	Noisy
SPR	24.10	19.64	0.9311	0.8840	0.0923	0.1702	12.03	65.25
NKSR	23.05	22.79	0.9307	0.9288	0.0964	0.1017	29.11	44.02
T.F.	26.12	26.01	0.9467	0.9436	0.0664	0.0711	6.83	8.21
Ours	26.29	26.26	0.9524	0.9516	0.0570	0.0574	4.90	4.93

4.3.2 **Quantitative comparisons.** We summarize the quantitative results in Tables 1 and 2. We can see that our method outperforms baselines on most metrics and datasets, especially on the two perceptual metrics FID and LPIPS with a significant margin. However, regarding PSNR, which prioritizes pixel-level accuracy and thus may differ from human perception of quality, our method is sometimes outperformed by SPR. We assume that SPR predicts a point’s color by somehow *fusing* nearby points’ colors, leading to blurry textures but safely avoiding extreme pixel-level errors. On the contrary, our method *dreams* the colors by its diffusion prior. While achieving visually better results, a few pixels with extremely high errors may lower the overall PSNR score.

4.4 Impact of Degraded Input Quality

4.4.1 **Anti-Noise Ability Analysis.** We compare the anti-noise abilities of our method and baseline methods by applying them on point clouds with manually added Gaussian noise (standard deviation = 0.005) from the chair category of ShapeNetCoreV2 dataset. Table 3 shows the results, where our method, even with noisy input, outperforms baselines with clean input, indicating a strong anti-noise ability. Visual comparisons can be found in our supplementary file.

4.4.2 **Sparsity Test.** To evaluate our method’s ability to deal with sparse input, we decrease the input point number from 30k to 20k gradually, and present the results in Table 4. We can see only a small performance drop, and even with only 20k points as input, our method outperforms baseline methods with 30k points as input; see results in Table 1 “Chairs” category. Again, visual comparisons can be found in our supplementary file.

4.5 Method Component Analysis

We here compare different implementations for sub-modules (geometry extraction, inpainting and unprojection module) of our method by replacing one module at a time while keeping others unchanged. All experiments in this subsection are conducted on the full test set of the chair category of ShapeNetCoreV2 dataset with Gaussian noise (standard deviation = 0.005).

4.5.1 **Geometry Extraction.** In addition to POCO, we further explore extracting geometry by SPR and depth inpainting to investigate how the geometry extraction module influence the final reconstructed textured mesh. Depth inpainting refers to inpainting projected sparse 2D depth maps instead of RGB images, and then reconstructing geometry from the inpainted dense depth maps by

Table 4: Comparisons on our method’s performance with increased input point cloud sparsity.

Point Number	PSNR \uparrow	SSIM \uparrow	LPIPS \downarrow	FID \downarrow
30k	26.2910	0.9524	0.0570	4.9048
25k	26.2761	0.9517	0.0580	5.2412
20k	26.2553	0.9509	0.0594	5.6960

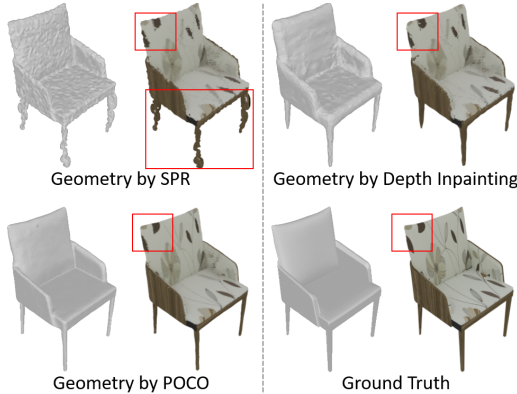


Figure 9: Geometry extraction module replacement results comparing our POCO against SPR and Depth Inpainting.



Figure 10: Inpainting module replacement results comparing our adopted DDNM against nearest interpolation, linear interpolation, and DiffPIR.

depth fusion [12]. Please refer to our supplementary file for more details and the quantitative results. We present the visual comparisons in Figure 9. We can see that, compared to POCO, both SPR and depth inpainting suffer from noisy geometry, resulting in noisy textures. Clearly, a higher-performance geometry extraction module contributes to a more refined reconstructed textured mesh.

4.5.2 2D Inpainting. We compare different inpainting modules in our pipeline, including nearest interpolation, linear interpolation, DiffPIR [63] and our adopted DDNM, where DiffPIR is another diffusion-based 2D image restoration method with inpainting ability. We provide the visual comparisons in Figure 10 and quantitative results in our supplementary file. As can be seen, the other three methods, though perform overall reasonably, fail to produce as clear textures as DDNM, indicating the importance of a strong inpainting module to the reconstruction performance.

4.5.3 Unprojection. We present the comparison results of different unprojection strategies in Figure 11 and Table 5.

- “Opt. Scratch” denotes optimizing the texture atlas from scratch [48];

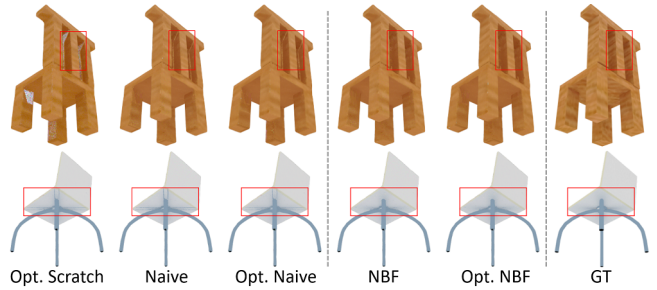


Figure 11: Qualitative results of replacing our unprojection strategy with others. “Opt.” denotes “Optimize”.

Table 5: Quantitative results of replacing our NBF unprojection strategy with others. “Opt.” denotes “Optimize”.

Unprojection Module	PSNR \uparrow	SSIM \uparrow	LPIPS \downarrow	FID \downarrow
Opt. Scratch [48]	26.1939	0.9473	0.0592	5.2619
Naive	26.2225	0.9500	0.0587	5.1068
Opt. Naive	26.2477	0.9511	0.0580	4.9389
NBF	26.2729	0.9512	0.0579	5.0309
Opt. NBF	26.2565	0.9516	0.0574	4.9326

- “Naive” selects the best views by direction priority;
- “NBF” selects the best views by our proposed Non-Border-First strategy;
- “Opt. Naive” further optimizes the obtained atlas of “Naive”;
- “Opt. NBF” further optimizes the obtained atlas of “NBF” while considering only loss in non-border areas.

The first row of Figure 11 shows an example, where optimizing from scratch fails on areas unseen from any view due to occlusion. Both rows show that the naive unprojection yields the above-mentioned artifacts from border areas, which can be slightly reduced by further optimization. Only our NBF and Opt. NBF nearly eliminate such artifacts. Table 5 also shows that our proposed NBF and Opt. NBF outperform other unprojection strategies.

5 CONCLUSION, LIMITATIONS AND FUTURE WORK

Conclusion. We propose PointDreamer, a novel zero-shot framework for textured mesh reconstruction from colored point cloud. PointDreamer predicts colors by 2D inpainting to utilize the strong diffusion prior and achieves SoTA performance. We also propose a novel “Non-Border-First” strategy to unproject the colors of predicted 2D images back to 3D space.

Limitation and Future Work. The main shortcoming of our proposed method is its relatively low speed. We employed one NVIDIA GeForce GTX 3090 GPU and it takes about 100s for our method to reconstruct a textured mesh, compared to NKSr’s 0.64 s. It takes about 72 s for DDNM [55] to inpaint our 8 multi-view images, which takes most of the time. Replacing DDNM with a faster inpainting module may increase our reconstruction speed. In the future, we may seek to address this issue, and further explore 3D-aware inpainting and relighting-supported texture reconstruction.

REFERENCES

- [1] Jonathan T. Barron, Ben Mildenhall, Matthew Tancik, Peter Hedman, Ricardo Martin-Brualla, and Pratul P. Srinivasan. 2021. Mip-NeRF: A Multiscale Representation for Anti-Aliasing Neural Radiance Fields. In *IEEE International Conference on Computer Vision (ICCV)*.
- [2] Alexandre Boulch and Renaud Marlet. 2022. POCO: Point Convolution for Surface Reconstruction. In *IEEE Conference on Computer Vision and Pattern Recognition (CVPR)*. 6302–6314.
- [3] Angel X Chang, Thomas Funkhouser, Leonidas Guibas, Pat Hanrahan, Qixing Huang, Zimo Li, Silvio Savarese, Manolis Savva, Shuran Song, Hao Su, et al. 2015. Shapenet: An information-rich 3d model repository. *arXiv preprint arXiv:1512.03012* (2015).
- [4] Rui Chen, Yongwei Chen, Ningxin Jiao, and Kui Jia. 2023. Fantasia3D: Disentangling Geometry and Appearance for High-quality Text-to-3D Content Creation. In *IEEE International Conference on Computer Vision (ICCV)*.
- [5] Zhiqin Chen, Kangxue Yin, and Sanja Fidler. 2022. AUV-Net: Learning Aligned UV Maps for Texture Transfer and Synthesis. In *IEEE Conference on Computer Vision and Pattern Recognition (CVPR)*.
- [6] Zhiqin Chen and Hao Zhang. 2019. Learning implicit fields for generative shape modeling. In *IEEE Conference on Computer Vision and Pattern Recognition (CVPR)*. 5939–5948.
- [7] Prafulla Dhariwal and Alexander Nichol. 2021. Diffusion models beat gans on image synthesis. *Advances in neural information processing systems* 34 (2021), 8780–8794.
- [8] Laura Downs, Anthony Francis, Nate Koenig, Brandon Kinman, Ryan Hickman, Krista Reymann, Thomas B McHugh, and Vincent Vanhoucke. 2022. Google scanned objects: A high-quality dataset of 3d scanned household items. In *International Conference on Robotics and Automation (ICRA)*. IEEE, 2553–2560.
- [9] Jun Gao, Tianchang Shen, Zian Wang, Wenzheng Chen, Kangxue Yin, Daiqing Li, Or Litany, Zan Gojcic, and Sanja Fidler. 2022. GET3D: A Generative Model of High Quality 3D Textured Shapes Learned from Images. In *Advances In Neural Information Processing Systems*.
- [10] Michael Garland and Paul S. Heckbert. 1997. Surface simplification using quadric error metrics. In *Proceedings of the 24th Annual Conference on Computer Graphics and Interactive Techniques (SIGGRAPH '97)*. ACM Press/Addison-Wesley Publishing Co., USA, 209–216. <https://doi.org/10.1145/258734.258849>
- [11] Shubham Goel, Angjoo Kanazawa, , and Jitendra Malik. 2020. Shape and Viewpoints without Keypoints. In *European Conference on Computer Vision (ECCV)*.
- [12] Griegler. 2017. *Pyfusion: a Python framework for volumetric depth fusion*. <https://github.com/griegler/pyfusion>
- [13] Anchit Gupta, Wenhan Xiong, Yixin Nie, Ian Jones, and Barlas Oğuz. 2023. 3DGen: Triplane Latent Diffusion for Textured Mesh Generation. *arXiv:2303.05371 [cs.CV]*
- [14] Martin Heusel, Hubert Ramsauer, Thomas Unterthiner, Bernhard Nessler, and Sepp Hochreiter. 2017. Gans trained by a two time-scale update rule converge to a local nash equilibrium. *Advances in neural information processing systems* 30 (2017).
- [15] Jonathan Ho, Ajay Jain, and Pieter Abbeel. 2020. Denoising diffusion probabilistic models. *Advances in neural information processing systems* 33 (2020), 6840–6851.
- [16] Tao Hu, Liwei Wang, Xiaogang Xu, Shu Liu, and Jiaya Jia. 2021. Self-Supervised 3D Mesh Reconstruction From Single Images. In *IEEE Conference on Computer Vision and Pattern Recognition (CVPR)*. 6002–6011.
- [17] Jiahui Huang, Zan Gojcic, Matan Atzmon, Or Litany, Sanja Fidler, and Francis Williams. 2023. Neural Kernel Surface Reconstruction. In *IEEE Conference on Computer Vision and Pattern Recognition (CVPR)*. 4369–4379.
- [18] Angjoo Kanazawa, Shubham Tulsiani, Alexei A. Efros, and Jitendra Malik. 2018. Learning Category-Specific Mesh Reconstruction from Image Collections. In *European Conference on Computer Vision (ECCV)*.
- [19] Sagi Katz, Ayellet Tal, and Ronen Basri. 2007. Direct Visibility of Point Sets. *ACM Transactions on Graphics* 26, 3 (jul 2007), 24–es. <https://doi.org/10.1145/1276377.1276407>
- [20] Michael Kazhdan, Matthew Bolitho, and Hugues Hoppe. 2006. Poisson surface reconstruction. In *Proceedings of the fourth Eurographics symposium on Geometry processing*, Vol. 7. 0.
- [21] Michael Kazhdan and Hugues Hoppe. 2013. Screened poisson surface reconstruction. *ACM Transactions on Graphics* 32, 3 (2013), 1–13.
- [22] Bernhard Kerbl, Georgios Kopanas, Thomas Leimkühler, and George Drettakis. 2023. 3D Gaussian Splatting for Real-Time Radiance Field Rendering. *ACM Transactions on Graphics* 42, 4 (July 2023). <https://repo-sam.inria.fr/fungraph/3d-gaussian-splatting/>
- [23] Samuli Laine, Janne Hellsten, Tero Karras, Yeongho Seol, Jaakko Lehtinen, and Timo Aila. 2020. Modular Primitives for High-Performance Differentiable Rendering. *ACM Transactions on Graphics* 39, 6 (2020).
- [24] Xueting Li, Sifei Liu, Kihwan Kim, Shalini De Mello, Varun Jampani, Ming-Hsuan Yang, and Jan Kautz. 2020. Self-supervised Single-view 3D Reconstruction via Semantic Consistency. In *European Conference on Computer Vision (ECCV)*.
- [25] Chen-Hsuan Lin, Jun Gao, Luming Tang, Towaki Takikawa, Xiaohei Zeng, Xun Huang, Karsten Kreis, Sanja Fidler, Ming-Yu Liu, and Tsung-Yi Lin. 2023. Magic3D: High-Resolution Text-to-3D Content Creation. In *IEEE Conference on Computer Vision and Pattern Recognition (CVPR)*.
- [26] Minghua Liu, Ruoxi Shi, Linghao Chen, Zhuoyang Zhang, Chao Xu, Xinyue Wei, Hansheng Chen, Chong Zeng, Jiayuan Gu, and Hao Su. 2023. One-2-3-45++: Fast Single Image to 3D Objects with Consistent Multi-View Generation and 3D Diffusion. *arXiv preprint arXiv:2311.07885* (2023).
- [27] Minghua Liu, Chao Xu, Haian Jin, Linghao Chen, Zexiang Xu, Hao Su, et al. 2023. One-2-3-45: Any single image to 3d mesh in 45 seconds without per-shape optimization. *arXiv preprint arXiv:2306.16928* (2023).
- [28] Ruoshi Liu, Rundi Wu, Basile Van Hoorick, Pavel Tokmakov, Sergey Zakharov, and Carl Vondrick. 2023. Zero-1-to-3: Zero-shot one image to 3d object. In *IEEE International Conference on Computer Vision (ICCV)*. 9298–9309.
- [29] Yuan Liu, Cheng Lin, Zijiao Zeng, Xiaoxiao Long, Lingjie Liu, Taku Komura, and Wenping Wang. 2024. SyncDreamer: Generating Multiview-consistent Images from a Single-view Image. In *International Conference on Learning Representations (ICLR)*.
- [30] Zhen Liu, Yao Feng, Michael J. Black, Derek Nowrouzezahrai, Liam Paull, and Weiyang Liu. 2023. MeshDiffusion: Score-based Generative 3D Mesh Modeling. In *International Conference on Learning Representations (ICLR)*.
- [31] Xiaoxiao Long, Yuan-Chen Guo, Cheng Lin, Yuan Liu, Zhiyang Dou, Lingjie Liu, Yuexin Ma, Song-Hai Zhang, Marc Habermann, Christian Theobalt, et al. 2023. Wonder3D: Single Image to 3D using Cross-Domain Diffusion. *arXiv preprint arXiv:2310.15008* (2023).
- [32] Luke Melas-Kyriazi, Christian Rupprecht, Iro Laina, and Andrea Vedaldi. 2023. RealFusion: 360 Reconstruction of Any Object from a Single Image. In *IEEE Conference on Computer Vision and Pattern Recognition (CVPR)*. <https://arxiv.org/abs/2302.10663>
- [33] Lars Mescheder, Michael Oechsle, Michael Niemeyer, Sebastian Nowozin, and Andreas Geiger. 2019. Occupancy Networks: Learning 3D reconstruction in function space. In *IEEE Conference on Computer Vision and Pattern Recognition (CVPR)*. 4460–4470.
- [34] Ben Mildenhall, Pratul P. Srinivasan, Matthew Tancik, Jonathan T. Barron, Ravi Ramamoorthi, and Ren Ng. 2020. NeRF: Representing Scenes as Neural Radiance Fields for View Synthesis. In *European Conference on Computer Vision (ECCV)*.
- [35] Thomas Müller, Alex Evans, Christoph Schied, and Alexander Keller. 2022. Instant Neural Graphics Primitives with a Multiresolution Hash Encoding. *ACM Transactions on Graphics* 41, 4, Article 102 (July 2022), 15 pages. <https://doi.org/10.1145/3528223.3530127>
- [36] Humza Naveed, Asad Ullah Khan, Shi Qiu, Muhammad Saqib, Saeed Anwar, Muhammad Usman, Naveed Akhtar, Nick Barnes, and Ajmal Mian. 2023. A Comprehensive Overview of Large Language Models. *arXiv:2307.06435 [cs.CL]*
- [37] Michael Oechsle, Lars Mescheder, Michael Niemeyer, Thilo Strauss, and Andreas Geiger. 2019. Texture Fields: Learning Texture Representations in Function Space. In *IEEE International Conference on Computer Vision (ICCV)*.
- [38] Jeong Joon Park, Peter Florence, Julian Straub, Richard Newcombe, and Steven Lovegrove. 2019. DeepSDF: Learning Continuous Signed Distance Functions for Shape Representation. In *IEEE Conference on Computer Vision and Pattern Recognition (CVPR)*.
- [39] Songyou Peng, Michael Niemeyer, Lars Mescheder, Marc Pollefeys, and Andreas Geiger. 2020. Convolutional occupancy networks. In *European Conference on Computer Vision (ECCV)*. Springer, 523–540.
- [40] Ben Poole, Ajay Jain, Jonathan T. Barron, and Ben Mildenhall. 2022. DreamFusion: Text-to-3D using 2D Diffusion. *arXiv* (2022).
- [41] Guocheng Qian, Jinjie Mai, Abdullah Hamdi, Jian Ren, Aliaksandr Siarohin, Bing Li, Hsin-Ying Lee, Ivan Skorokhodov, Peter Wonka, Sergey Tulyakov, and Bernard Ghanem. 2024. Magic123: One Image to High-Quality 3D Object Generation Using Both 2D and 3D Diffusion Priors. In *International Conference on Learning Representations (ICLR)*.
- [42] Iqbal H Sarker. 2021. Deep learning: a comprehensive overview on techniques, taxonomy, applications and research directions. *SN Computer Science* 2, 6 (2021), 420.
- [43] Tianchang Shen, Jun Gao, Kangxue Yin, Ming-Yu Liu, and Sanja Fidler. 2021. Deep Marching Tetrahedra: a Hybrid Representation for High-Resolution 3D Shape Synthesis. In *Advances in Neural Information Processing Systems (NeurIPS)*.
- [44] Ruoxi Shi, Hansheng Chen, Zhuoyang Zhang, Minghua Liu, Chao Xu, Xinyue Wei, Linghao Chen, Chong Zeng, and Hao Su. 2023. Zero123++: A Single Image to Consistent Multi-view Diffusion Base Model. *arXiv:2310.15110 [cs.CV]*
- [45] Jingxiang Sun, Bo Zhang, Ruizhi Shao, Lizhen Wang, Wen Liu, Zhenda Xie, and Yebin Liu. 2023. DreamCraft3D: Hierarchical 3D Generation with Bootstrapped Diffusion Prior. In *International Conference on Learning Representations (ICLR)*.
- [46] Stanislaw Szymanowicz, Christian Rupprecht, and Andrea Vedaldi. 2023. Viewset Diffusion: (0-)Image-Conditioned 3D Generative Models from 2D data. In *IEEE International Conference on Computer Vision (ICCV)*.
- [47] Jiapeng Tang, Jiabao Lei, Dan Xu, Feiying Ma, Kui Jia, and Lei Zhang. 2021. Sa-ConvNet: Sign-agnostic optimization of convolutional occupancy networks. In *IEEE International Conference on Computer Vision (ICCV)*. 6504–6513.

- [48] Jiaxiang Tang, Jiawei Ren, Hang Zhou, Ziwei Liu, and Gang Zeng. 2023. Dream-Gaussian: Generative Gaussian Splatting for Efficient 3D Content Creation. *arXiv preprint arXiv:2309.16653* (2023).
- [49] Junshu Tang, Tengfei Wang, Bo Zhang, Ting Zhang, Ran Yi, Lizhuang Ma, and Dong Chen. 2023. Make-It-3D: High-fidelity 3D Creation from A Single Image with Diffusion Prior. In *IEEE International Conference on Computer Vision (ICCV)*. 22819–22829.
- [50] Jiaxiang Tang, Hang Zhou, Xiaokang Chen, Tianshu Hu, Errui Ding, Jingdong Wang, and Gang Zeng. 2023. Delicate Textured Mesh Recovery from NeRF via Adaptive Surface Refinement. In *IEEE International Conference on Computer Vision (ICCV)*. 17739–17749.
- [51] Fei Tao, Bin Xiao, Qinglin Qi, Jiangfeng Cheng, and Ping Ji. 2022. Digital twin modeling. *Journal of Manufacturing Systems* 64 (2022), 372–389.
- [52] Gabriel Taubin. 1995. A signal processing approach to fair surface design. In *Proceedings of the 22nd Annual Conference on Computer Graphics and Interactive Techniques (SIGGRAPH '95)*. Association for Computing Machinery, New York, NY, USA, 351–358. <https://doi.org/10.1145/218380.218473>
- [53] Guangyu Wang, Jinzhi Zhang, Fan Wang, Ruqi Huang, and Lu Fang. 2024. XScale-NVS: Cross-Scale Novel View Synthesis with Hash Featurized Manifold. *arXiv:2403.19517 [cs.CV]*
- [54] Yuntao Wang, Zhou Su, Ning Zhang, Rui Xing, Dongxiao Liu, Tom H Luan, and Xuemin Shen. 2022. A survey on metaverse: Fundamentals, security, and privacy. *IEEE Communications Surveys & Tutorials* 25, 1 (2022), 319–352.
- [55] Yinhuai Wang, Jiwen Yu, and Jian Zhang. 2022. Zero-Shot Image Restoration Using Denoising Diffusion Null-Space Model. In *International Conference on Learning Representations (ICLR)*.
- [56] Zhou Wang, Alan C Bovik, Hamid R Sheikh, and Eero P Simoncelli. 2004. Image quality assessment: from error visibility to structural similarity. *IEEE Transactions on Image Processing* 13, 4 (2004), 600–612.
- [57] Xingkui Wei, Zhengqing Chen, Yanwei Fu, Zhaopeng Cui, and Yinda Zhang. 2021. Deep Hybrid Self-Prior for Full 3D Mesh Generation. In *IEEE International Conference on Computer Vision (ICCV)*. 5805–5814.
- [58] Tong Wu, Jiarui Zhang, Xiao Fu, Yuxin Wang, Jiawei Ren, Liang Pan, Wayne Wu, Lei Yang, Jiaqi Wang, Chen Qian, Dahua Lin, and Ziwei Liu. 2023. OmniObject3D: Large-Vocabulary 3D Object Dataset for Realistic Perception, Reconstruction and Generation. In *IEEE Conference on Computer Vision and Pattern Recognition (CVPR)*.
- [59] Jonathan Young. 2022. Xatlas: Mesh parameterization / UV unwrapping library. <https://github.com/jpcy/xatlas> 3.
- [60] Junzhe Zhang, Daxuan Ren, Zhongang Cai, Chai Kiat Yeo, Bo Dai, and Chen Change Loy. 2022. Monocular 3D Object Reconstruction with GAN Inversion. In *European Conference on Computer Vision (ECCV)*.
- [61] Richard Zhang, Phillip Isola, Alexei A Efros, Eli Shechtman, and Oliver Wang. 2018. The unreasonable effectiveness of deep features as a perceptual metric. In *IEEE Conference on Computer Vision and Pattern Recognition (CVPR)*. 586–595.
- [62] Xin-Yang Zheng, Hao Pan, Peng-Shuai Wang, Xin Tong, Yang Liu, and Heung-Yeung Shum. 2023. Locally Attentional SDF Diffusion for Controllable 3D Shape Generation. *ACM Transactions on Graphics (SIGGRAPH)* 42, 4 (2023).
- [63] Yuanzhi Zhu, Kai Zhang, Jingyun Liang, Jiezhang Cao, Bihan Wen, Radu Timofte, and Luc Van Gool. 2023. Denoising Diffusion Models for Plug-and-Play Image Restoration. In *IEEE Conference on Computer Vision and Pattern Recognition Workshops (NTIRE)*.

A APPENDIX: IMPLEMENTATION DETAILS

A.1 Texture Field Baseline

A.1.1 Network architecture. Inspired by works [13, 43] that represent 3D information by a feature tri-plane, we adopt the network architecture of the open-source Convolutional Occupancy Network [39], which also follows a tri-plane representation. Specifically, we modify its one-dimensional output head for occupancy prediction to three-dimensional for RGB color prediction.

A.1.2 Training. We follow 3DGen [13] to train the network by the per-3D-point MSE loss on predicted and GT colors of sampled 3D points. Additionally, we also tried to employ the per-2D-pixel MSE loss of 2D images rendered from GT meshes and predicted meshes by differentiable rendering, but the experimental results are worse, as shown in Figure 12. Therefore, we adopt the per-3D-point MSE loss in our manuscript. We train the texture field network on a single NVIDIA GeForce GTX 3090 GPU with a batch size of 24 and a learning rate of 0.0001 for 2592, 024 iterations (about 356 epochs).

A.1.3 Inference. During inference, we first use POCO [2] to predict an untextured mesh from the input point cloud, and apply UV mapping to it by Xatlas [59], which produces the 3D positions of each valid pixel in the texture atlas. We query the color of each of these 3D positions by our trained texture field network, to inpaint the texture atlas, so as to obtain the final textured mesh.

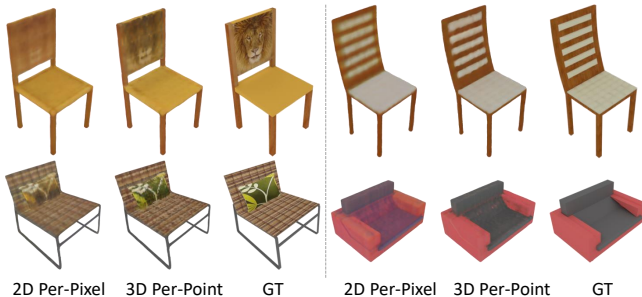


Figure 12: Visual comparisons of the Texture Field baseline trained with different losses. “2D per-pixel” denotes rendering the generated textured mesh to multi-view 2D images, and then calculating the MSE loss between the rendered and GT images. “3D per-point” denotes calculating MSE loss between the predicted and GT colors of sampled 3D points.

A.2 Depth Inpainting for Geometry Extraction

With 2D inpainting adopted as the key for our texture reconstruction, we can also introduce it to geometry reconstruction, by inpainting 2D depth maps instead of RGB images. Specifically, we follow the following steps to reconstruct untextured meshes from the input point cloud, as shown in Figure 13:

- (1) We generate multi-view sparse depth maps by projecting 3D points to 2D, and assigning the value of each pixel as the depth value of the corresponding 3D point. Note that, similar to generating our sparse RGB images, hidden point removal is conducted for each viewpoint before projecting.

- (2) Since depth fusion requires depth maps’ background pixels to have infinite values to produce a reasonable mesh, we generate foreground masks by projecting 3D points to 2D space with a relatively big point size, i.e. the number of 2D pixels occupied by each 3D point. In this way, most foreground pixels (pixels that should correspond to a point on the 3D mesh) can be occupied, and we use the closing operation of morphology to fill the rest small holes. In addition, since we use a big point size to generate the foreground mask, the mask would be bigger than the ground truth, so we shrink the generated mask by erosion.
- (3) We inpaint the foreground pixels of the sparse depth maps into dense ones by nearest interpolation considering efficiency.
- (4) We produce an untextured mesh by depth fusion based on the inpainted dense depth maps, and conduct mesh simplification [10] and Taubin Smooth [52] to it as post-processing, to get the final untextured mesh.

B APPENDIX: MORE EXPERIMENTAL RESULTS

B.1 Effect of Different K Values (Number of Viewpoints for Projection and Inpainting)

To investigate the effect of different numbers of viewpoints (denoted as K) for projection and inpainting, we conduct experiments on the motorbike category or ShapeNetCoreV2 dataset by using different K values including 6, 8, and 20. Table 6 shows the distribution of cameras for each setting, together with the quantitative results. We can see that more views contribute to a slightly higher reconstruction quality. Visual comparisons in Figure 14 also show that, an insufficient number of views would produce artifacts in invisible or occluded areas, thus impacting the performance.

Considering that using $K = 20$ views is only slightly better than setting $K = 8$, but inpainting more views’ images can be much more time-consuming, we set the number of views to be 8 for most datasets in our manuscript to balance both effectiveness and efficiency. The only exception is the motorbike category from the ShapeNetCoreV2 dataset, for which we use the 20 views instead, considering motorbikes’ more complex geometry and topology.

B.2 Visual Comparisons: Impact of Degraded Input Quality

B.2.1 Anti-Noise Ability Analysis. Figure 15 presents the visual comparisons of our method and baseline methods’ reconstructed meshes from noisy or clean input point clouds. Overall, we have the following observations, which are consistent with the quantitative results in our manuscript:

- (1) As expected, all methods produce higher-quality textured meshes with clean input point clouds compared to noisy ones.
- (2) Our PointDreamer shows a relatively high anti-noise ability, where only a small performance drop is observed when giving noisy input.

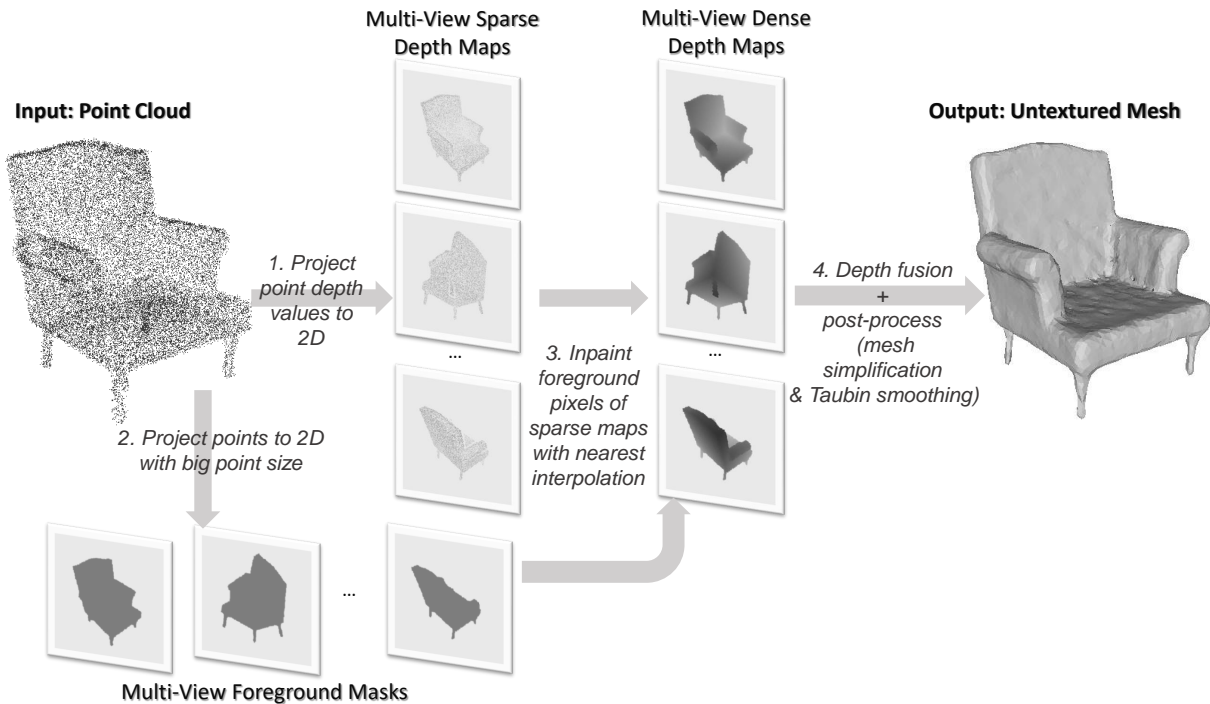


Figure 13: Pipeline of extracting geometry by depth inpainting.

Table 6: Quantitative results of using different K values (numbers of viewpoints for projection and inpainting) on the motorbike category of ShapeNetCoreV2 dataset. More views contribute to a slightly higher reconstruction quality.

Viewpoint Number	Camera Distribution	PSNR \uparrow	SSIM \uparrow	LPIPS \downarrow	FID \downarrow
6	At the centers of each face of a cube	20.8755	0.9273	0.0585	33.2870
8	Evenly distributed on a Fibonacci Sphere	21.0664	0.9287	0.0572	30.2113
20	On the 20 vertices of a regular icosahedron	21.2013	0.9299	0.0562	28.4213

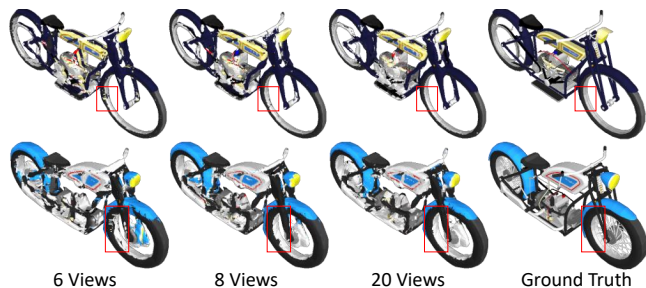


Figure 14: Visual comparisons of our reconstructed meshes with different K values (numbers of viewpoints for projection and inpainting). An insufficient number of views would lead to artifacts in invisible or occluded areas.

- (3) Our PointDreamer with noisy input point clouds shows an even better visual effect compared to baseline methods with clean inputs.

B.2.2 Sparsity Test. Figure 16 shows the visual comparisons of our PointDreamer’s reconstructed meshes with different numbers of points as input. There is a very small performance drop introduced by decreasing the input point number, which can sometimes be hard to notice by human eyes. This indicates a relatively high robustness of our method towards varying degrees of input sparsity.

B.3 Quantitative Results of Method Component Analysis

B.3.1 Geometry Extraction. We provide the quantitative results of replacing our geometry extraction module from POCO to SPR and Depth Inpainting in Table 7. As can be seen, POCO, as a state-of-the-art deep-learning-based surface reconstruction approach, outperforms the other two methods by a significant margin, especially regarding FID. This is consistent with the visual comparisons (see Figure 9) in our manuscript where both SPR and Depth Inpainting suffer from noisy geometry and thus low-quality textures.

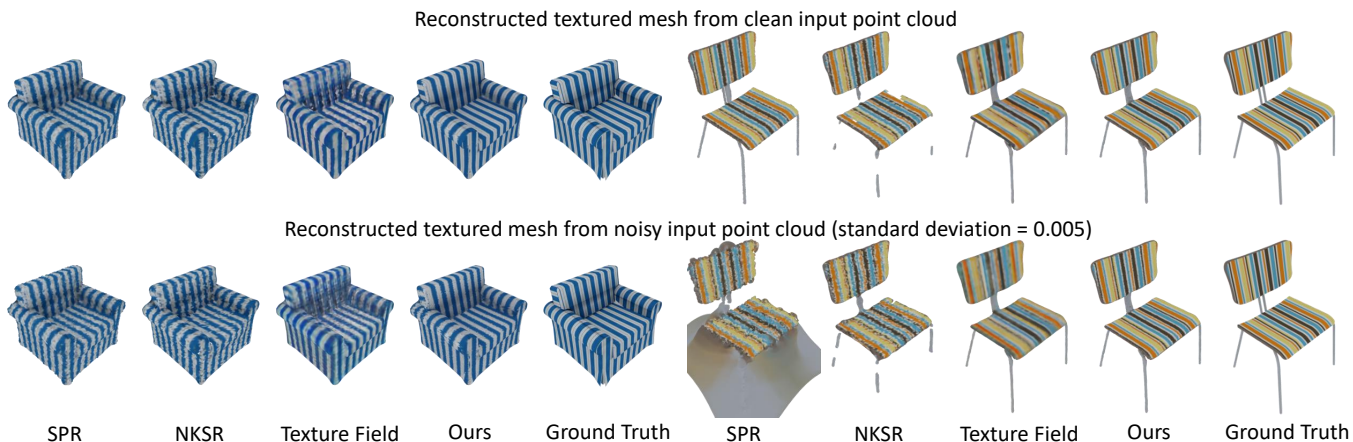


Figure 15: Visual comparisons of our PointDreamer’s and baseline methods’ reconstructed meshes, with noisy or clean point clouds as input. Our PointDreamer shows a strong anti-noise ability by producing high-quality textures even with noisy input.

Table 8: Quantitative results of replacing our inpainting module from DDNM to nearest interpolation, linear interpolation, and DiffPIR.

Inpainting Module	PSNR \uparrow	SSIM \uparrow	LPIPS \downarrow	FID \downarrow
Nearest Interpolation	26.1175	0.9457	0.0618	11.0205
Linear Interpolation	26.1739	0.9474	0.0612	9.4725
DiffPIR	26.1582	0.9456	0.0652	9.4823
Our Adopted DDNM	26.2565	0.9516	0.0574	4.9326

Table 7: Quantitative results of replacing our geometry extraction module from POCO to SPR and Depth Inpainting.

Geometry Module	PSNR \uparrow	SSIM \uparrow	LPIPS \downarrow	FID \downarrow
SPR	19.4071	0.8752	0.1777	74.9854
Depth Inpainting	26.2502	0.9466	0.0717	20.7198
Our Adopted POCO	26.2565	0.9516	0.0574	4.9326

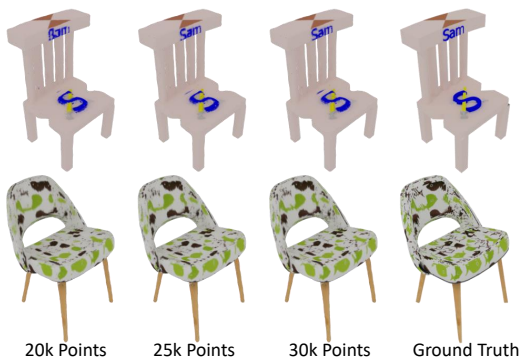


Figure 16: Visual comparisons of our PointDreamer’s reconstructed meshes with different numbers of points as input. There is a small performance drop when adopting sparser input, which sometimes can be hard to notice by human eyes.

B.3.2 2D Inpainting. We provide the quantitative results of replacing our 2D inpainting module from DDNM [55] to nearest interpolation, linear interpolation, and DiffPIR [63] in Table 8. DiffPIR is another 2D-diffusion-based image restoration approach with inpainting ability. As can be seen, DDNM outperforms the other three methods thanks to its strong inpainting ability, which is consistent with the visual comparisons (see Figure 10) in our manuscript.